Supporting Information

Sensitivity-Enhanced Four-Dimensional Amide—Amide Correlation NMR Experiments for Sequential Assignment of Proline-Rich Disordered Proteins

Leo E. Wong,* Joachim Maier, Jürgen Wienands, Stefan Becker, Christian Griesinger*

Proline is prevalent in intrinsically disordered proteins (IDPs). NMR assignment of proline-rich IDPs is a challenge due to low dispersion of chemical shifts. We propose here new sensitivity-enhanced 4D NMR experiments that correlate two pairs of amide resonances that are either consecutive (NH_{i-1}, NH_i) or flanking a proline at position *i*-1 (NH_{i-2}, NH_i). The maximum 2-fold enhancement of sensitivity is achieved by employing two coherence order-selective (COS) transfers incorporated unconventionally into the pulse sequence. Each COS transfer confers an enhancement over amplitude-modulated transfer by a factor of √2 specifically when transverse relaxation is slow. The experiments connect amide resonances over a long fragment of sequence interspersed with proline. When this method was applied to the proline-rich region of B cell adaptor protein SLP-65 (pH 6.0) and α-synuclein (pH 7.4), which contain a total of 52 and 5 prolines, respectively, 99 % and 92 % of their nonprolyl amide resonances have been successfully assigned, demonstrating its robustness to address the assignment problem in large proline-rich IDPs.

Table of Contents

1.	**General principle of sensitivity enhancement by coherence order-selective transfers**	**pg. S3-S4**
2.	**Pulse sequences of sensitivity-enhanced HNcocaNH and HNcocancaNH**	**pg. S5-S6**
3.	**Instructions for running the experiments on TopSpin in APSY approach**	**pg. S7-S8**
4.	**Protein expression and sample preparation**	**pg. S9**
5.	**List of NMR experiments and acquisition parameters**	**pg. S10-S11**
6.	**Other supporting figures**	**pg. S12-S15**
7.	**References**	**pg. S15**

1. General principle of sensitivity enhancement by coherence order-selective transfers

There are two types of coherence transfers between chemical shift evolution periods t_j and t_{j+1}.

Amplitude-modulated (AM) coherence transfer:

$$\cos(\Omega_j t_j)\, e^{+i\Omega_{j+1} t_{j+1}} \text{ or } \sin(\Omega_j t_j)\, e^{+i\Omega_{j+1} t_{j+1}} \qquad (1)$$

Coherence order-selective (COS) transfer:

$$e^{+i\Omega_j t_j} e^{+i\Omega_{j+1} t_{j+1}} \text{ or } e^{-i\Omega_j t_j} e^{+i\Omega_{j+1} t_{j+1}} \qquad (2)$$

Let's assume the S/N of a FID to be η. In AM transfer, the signal is modulated by either sine or cosine function in dimension *j*, thus signal intensity will be divided between two peaks at $+\Omega_j$ and $-\Omega_j$ in the frequency domain. After addition of the two FIDs for sign discrimination, the overall S/N becomes (√2/2)*η. In COS transfer, the signal is modulated by either $e^{+i\Omega_j t_j}$ or $e^{-i\Omega_j t_j}$, thus only a single peak exists at either $+\Omega_j$ or $-\Omega_j$ in the frequency domain. However, both "echo" and "anti-echo" FIDs are acquired to generate pure absorption peaks via the Rance-Kay procedure[1-3]. Anti-echo refers to signal with the same sign of frequency modulation, while echo is the opposite. The overall S/N becomes 1*η after processing. Therefore, every COS transfer enhances the sensitivity by a factor of √2 over AM transfer.

In an *n*D experiment, the maximum enhancement in sensitivity depends on the numbers of COS transfers, irrespective of the order of combination to AM transfer (Figure 1 in Main Text). Consider an experiment that starts with Cartesian operator I_x and goes through multiple COS transfers between evolution of single-quantum coherences until period t_k, after which an AM transfer is introduced between period t_k and t_{k+1}. At the beginning, after the first evolution period, the density operator can be represented by raising and lowering operators as $\frac{1}{2}\left(I_+ e^{-i\Omega_1 t_1} + I_- e^{+i\Omega_1 t_1}\right)$. After going through multiple COS transfers and at the end of evolution period t_k, operators I_+ and I_- are modulated by $e^{-i\Theta}$ and $e^{+i\Theta}$, respectively, where $\Theta = \Omega_k t_k \pm \Omega_{k-1} t_{k-1} \ldots \pm \Omega_1 t_1$. The "+" or "−" sign between each chemical shift term depends on whether it is echo or anti-echo transfer for the individual COS transfer. The two complex modulations can be converted by Euler's formula to $\cos\Theta \mp i \sin\Theta$, and the density operator becomes $I_x \cos\Theta + I_y \sin\Theta$. Subsequent AM transfer selects Cartesian operators I_x or I_y, which is amplitude-modulated by $\cos\Theta$ and $\sin\Theta$, respectively. Following the argument in the first paragraph, the overall sensitivity for the sign-discriminated peak will be reduced by √2 only, after Fourier transform and proper processing from dimension 1 to *k*. In a less mathematical way, one can formulate this phenomenon in the following way: since evolution occurs during period t_k, I_x is amplitude-modulated by a superposition of the amplitudes of I_x and I_y before the evolution begins. Hence, the accumulated complex modulation is being propagated successfully.

For proper processing, echo/anti-echo and sine/cosine FIDs are recorded for each COS and AM transfer, respectively. The FIDs have to be recombined in a specific way depending on the order of combination of COS and AM transfers. The way to recombine the FIDs for a particular *n*D experiment can be determined by expanding $\cos\Theta$ and $\sin\Theta$, at the point when a train of COS transfers is followed by an AM transfer. For example, in the case of the sensitivity-enhanced 4D amide-amide correlation experiments with two COS transfers:

FID no.	t_1 -> t_2 -> t_3 -> t_4
S1	echo – cosine – echo
S2	antiecho – cosine – echo
S3	echo – sine – echo
S4	antiecho – sine – echo
S5	echo – cosine – antiecho
S6	antiecho – cosine – antiecho
S7	echo – sine – antiecho
S8	antiecho – sine – antiecho

The way to recombine the FIDs is as follows:

S1 + S2 + S5 + S6	$\cos(\Omega_1 t_1)*\cos(\Omega_2 t_2)*\cos(\Omega_3 t_3)*e^{(i\Omega 4t4)}$
S3 – S4 + S7 – S8	$\sin(\Omega_1 t_1)*\cos(\Omega_2 t_2)*\cos(\Omega_3 t_3)*e^{(i\Omega 4t4)}$
S3 + S4 + S7 + S8	$\cos(\Omega_1 t_1)*\sin(\Omega_2 t_2)*\cos(\Omega_3 t_3)*e^{(i\Omega 4t4)}$
– S1 + S2 – S5 + S6	$\sin(\Omega_1 t_1)*\sin(\Omega_2 t_2)*\cos(\Omega_3 t_3)*e^{(i\Omega 4t4)}$
– *i**(S1 + S2 – S5 – S6)	$\cos(\Omega_1 t_1)*\cos(\Omega_2 t_2)*\sin(\Omega_3 t_3)*e^{(i\Omega 4t4)}$
– *i**(S3 – S4 – S7 + S8)	$\sin(\Omega_1 t_1)*\cos(\Omega_2 t_2)*\sin(\Omega_3 t_3)*e^{(i\Omega 4t4)}$
– *i**(S3 + S4 – S7 – S8)	$\cos(\Omega_1 t_1)*\sin(\Omega_2 t_2)*\sin(\Omega_3 t_3)*e^{(i\Omega 4t4)}$
– *i**(– S1 + S2 + S5 – S6)	$\sin(\Omega_1 t_1)*\sin(\Omega_2 t_2)*\sin(\Omega_3 t_3)*e^{(i\Omega 4t4)}$

For the purpose of pulse sequence design, it is convenient to follow the experiment in Cartesian operators. Using the refocused INEPT sequence for COS transfer, it is flexible to transform I_x to $\pm J_x$ or $\pm J_y$, and I_y to $\pm J_y$ or $\pm J_x$, where $\pm I_{x,y}$ and $\pm J_{x,y}$ are the Cartesian operators before and after the transfer. Different forms of density operator (represented by raising and lowering operators) will be obtained at the end of the evolution period after the transfer in different scenarios. Assuming that the experiment starts as I_x, the following table provides a guideline on the form of density operator obtained after the transfer and evolution. Naturally, it is sufficient to repeatedly employ rules I and III to obtain the required echo and antiecho FIDs for any *n*D experiment.

	Transformation scenarios		**Density operator**	$\boldsymbol{J_x\cos\Theta + J_y\sin\Theta}$	
I	$I_x \rightarrow J_x$	$I_y \rightarrow J_y$	$\frac{1}{2}\left(I_+ e^{-i\Theta} + I_- e^{+i\Theta}\right)$	$\Theta = \Omega_2 t_2 + \Omega_1 t_1$	Echo*
II	$I_x \rightarrow -J_x$	$I_y \rightarrow J_y$	$-\frac{1}{2}\left(I_+ e^{-i\Theta} + I_- e^{+i\Theta}\right)$	$\Theta = \Omega_2 t_2 - \Omega_1 t_1$	Antiecho*
III	$I_x \rightarrow J_x$	$I_y \rightarrow -J_y$	$\frac{1}{2}\left(I_+ e^{-i\Theta} + I_- e^{+i\Theta}\right)$	$\Theta = \Omega_2 t_2 - \Omega_1 t_1$	Antiecho
IV	$I_x \rightarrow -J_x$	$I_y \rightarrow -J_y$	$-\frac{1}{2}\left(I_+ e^{-i\Theta} + I_- e^{+i\Theta}\right)$	$\Theta = \Omega_2 t_2 + \Omega_1 t_1$	Echo
V	$I_x \rightarrow J_y$	$I_y \rightarrow J_x$	$-\frac{i}{2}\left(I_+ e^{-i\Theta} - I_- e^{+i\Theta}\right)$	$\Theta = \Omega_2 t_2 - \Omega_1 t_1$	Antiecho
VI	$I_x \rightarrow -J_y$	$I_y \rightarrow J_x$	$\frac{i}{2}\left(I_+ e^{-i\Theta} - I_- e^{+i\Theta}\right)$	$\Theta = \Omega_2 t_2 + \Omega_1 t_1$	Echo
VII	$I_x \rightarrow J_y$	$I_y \rightarrow -J_x$	$-\frac{i}{2}\left(I_+ e^{-i\Theta} - I_- e^{+i\Theta}\right)$	$\Theta = \Omega_2 t_2 + \Omega_1 t_1$	Echo
VIII	$I_x \rightarrow -J_y$	$I_y \rightarrow -J_x$	$\frac{i}{2}\left(I_+ e^{-i\Theta} - I_- e^{+i\Theta}\right)$	$\Theta = \Omega_2 t_2 - \Omega_1 t_1$	Antiecho

*This is an echo (antiecho) transfer, if coherence transfer between ^{1}H and ^{15}N is considered, in which ^{15}N spin has a negative gyromagnetic ratio and therefore Ω_1 and Ω_2 have different signs.

2. Pulse sequences of sensitivity-enhanced HNcocaNH and HNcocancaNH (x-P-x)

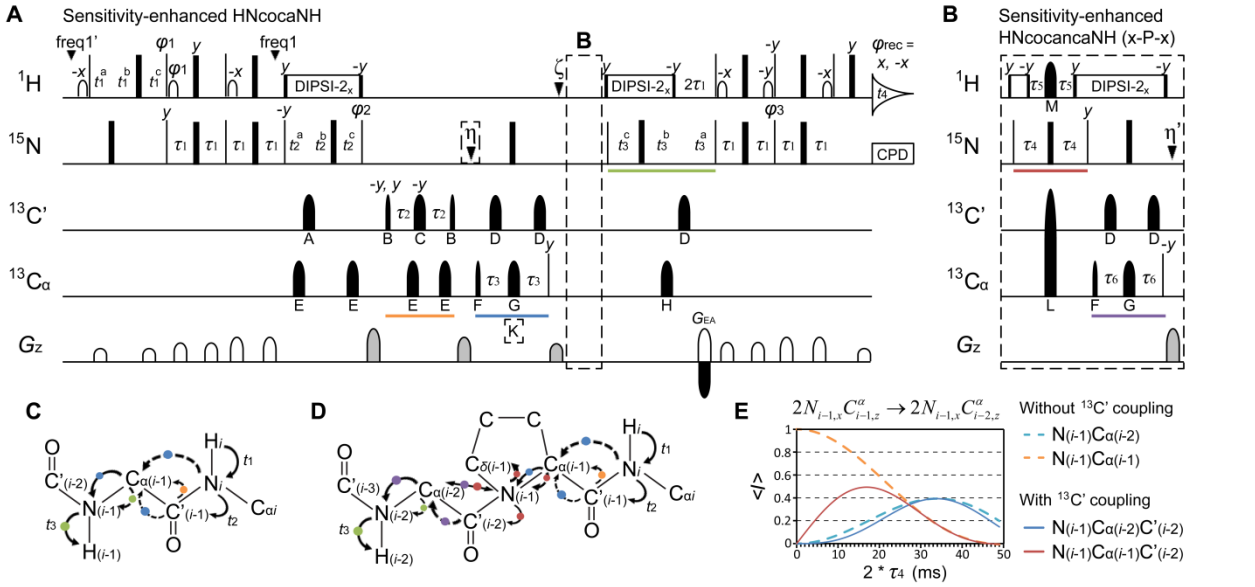

Figure S1. Pulse sequences of sensitivity-enhanced 4D amide-amide correlation NMR experiments. (A) Pulse sequence of sensitivity-enhanced 4D HNcocaNH experiment. Narrow and wide rectangular bars represent nonselective 90° and 180° pulses, respectively. ^{1}H carrier frequency is shifted from freq1' = 8.2 ppm to freq1 = 4.7 ppm (H_2O's offset). Carrier frequencies for hard pulses on ^{15}N and ^{13}C channels are 120 ppm and 56 ppm, respectively, while shaped pulses on ^{13}C' are centered at 176 ppm. Shaped pulse on ^{1}H is 90° water flip-back pulse of 1.3 ms. Decoupling on ^{1}H and ^{15}N was performed using DIPSI-2 and WALTZ-16, respectively. Shaped pulses on ^{13}C with their respective pulse lengths determined for 700 MHz spectrometer are summarized as follows: A (rectangle, 40.9 μs), B (Gauss 5%, 120 μs), C (Q3, 240 μs), D (I3Snob, 200 μs), E (IBurp2, 300 μs, 45 ppm), F (EBurp2, 200 μs, 56 ppm), G (Reburp, 330 μs, 45 ppm), and H (rectangle, 40.9 μs, 56 ppm). Pulses without indication of a phase above the pulse symbol were applied with phase x. φ_1 = y and is inverted for echo/antiecho selection. φ_2 = x and is shifted to y for sine/cosine selection. φ_3 = y and is inverted for echo/antiecho selection. The respective FIDs are recombined in a specific way as detailed in Section 1 of the Supporting Information. The sign of pulsed field gradient G_{EA} is inverted together with phase φ_3. Gradients for purging purpose are colored gray. Fixed delays are τ_1 = 2.7 ms, τ_2 = 4.75 ms, and τ_3 = 27 ms. All indirect dimensions were sampled in constant-time or semi-constant-time fashion[4]. The following initial delays were used: $t_1^a = t_1^c$ = 2.7 ms, $t_2^a = t_2^c$ = 14 ms, $t_3^a = t_3^c$ = 14 ms, while $t_1^b = t_2^b = t_3^b$ = 0 ms. Time point ζ is discussed in the text. Colored lines represent periods during which the magnetization transfer pathways as depicted in (C) and (D) are active. (B) The sensitivity-enhanced 4D HNcocancaNH (x-P-x) experiment is built up from (A) by inserting two additional magnetization transfer blocks after time point ζ. Time point η indicates the position to switch ^{15}N carrier frequency to 127 ppm to accommodate amide of proline, which will be switched back after η'. Other ^{13}C shaped pulses include K (Q3, 750 μs, 64 ppm) and L (Chirp60, 400 μs, 110 ppm). Proton shaped pulse M (I3Snob, 1.3 ms) is centered at 8.5 ppm. Fixed delay τ_3 right after η (blue line) is changed to 24 ms, while τ_4 = 16.5 ms (red line) and τ_6 = 27 ms (purple line). τ_5 is adjusted to 2.5 ms to account for scalar coupling during shaped pulse M. (C and D) Magnetization transfer pathways for experiments (A) and (B), respectively, that correlate two pairs of amide ^{1}H–^{15}N resonances that are either consecutive (NH_{i-1}, NH_i) or flanking a proline at position i-1 (NH_{i-2}, NH_i). Transfer pathways that

are occurring during the same evolution period are denoted by the same color. Refocusing pathways are indicated by dashed arrows. (E) The expectation values of different coherences evolving during the period of 2 times τ_4 in (B) for the transfer pathway of $2N_{i-1,x}C^{\alpha}_{i-1,z} \rightarrow 2N_{i-1,x}C^{\alpha}_{i-2,z}$ are plotted for two scenarios, *i.e.* with and without coupling to ^{13}C'. The calculation was done based on the following scalar coupling constants: ^{1}J(N,C$^{\alpha}$) = 10.7 Hz, ^{2}J(N,C$^{\alpha}$) = 7.7 Hz, ^{1}J(N,C') = 15 Hz, and ^{1}J(N,C$^{\delta}$) = 8.8 Hz.

The first 4D experiment (Figures S1A and C) that correlates two adjacent amides is a sensitivity-enhanced version incorporating two COS transfers into a sequence from Fiorito *et al.*[4]. The second 4D experiment (Figures S1B and D) contains two additional transfer steps to connect two amides (NH_{i-2}, NH_i) whose amino acids are separated by a proline. At point ζ, we have two-spin order of prolyl $^{15}N_{(i-1)}$ and $^{13}C^{\alpha}_{(i-1)}$. During the subsequent evolution period, prolyl $^{15}N_{(i-1)}$'s coupling to $^{13}C^{\alpha}_{(i-2)}$ generates anti-phase coherence with $^{13}C^{\alpha}_{(i-2)}$, while its anti-phase coherence with $^{13}C^{\alpha}_{(i-1)}$ is refocused. Concurrently, prolyl $^{15}N_{(i-1)}$ is also coupled to $^{13}C^{\delta}_{(i-1)}$ and $^{13}C'_{(i-2)}$ – a design that serves two purposes. First, it is difficult to selectively decouple $^{13}C^{\delta}$ without loss, since the chemical shift of $^{13}C^{\delta}$ is distributed in a narrow gap between $^{13}C^{\alpha}$ of glycine and the remaining amino acids. We measured the ^{1}J(N,C$_{\delta}$) coupling constant to be 8.8 ± 0.3 Hz. As a result of this coupling, efficiency of the targeted transfer to $^{13}C^{\alpha}_{(i-2)}$ is limited to about 40 % at maximum by setting the period of two times τ_4 to 33 milliseconds (Figures S1B and E). Meanwhile, refocusing of $^{13}C^{\alpha}_{(i-1)}$ anti-phase coherence is also incomplete (Figure S1E). To prevent detection of back-transferred amide coherence, $^{13}C'_{(i-2)}$ is coupled to prolyl $^{15}N_{(i-1)}$, which is then refocused after the transfer to $^{13}C^{\alpha}_{(i-2)}$. The 40 % transfer efficiency is maintained in spite of simultaneous coupling to $^{13}C'_{(i-2)}$ (Figure S1E). Lastly, this is a clean experiment that detects exclusively amides flanking a proline, since amide ^{1}J(N,H) coupling is active during the same evolution period and will be crushed by gradient afterwards (Figure S1B).

3. Instructions for running the experiments on TopSpin in APSY approach

So far, the experiments have not yet been incorporated into Bruker's TopSpin AU or GUI for APSY, and thus, users who run the provided pulse program directly will have to follow these instructions.

Projection of a 4D experiment into 2D spectrum with projection angles α and β not equal to 0° or 90° will give a total of four 2D projection spectra: (+α, +β), (-α, +β), (+α, -β) and (-α, -β)[5,6]. The acquired FIDs for each set of projection angles will be stored as the "parent" dataset, after which the four "child" datasets can be generated by the python script *apsy_HNMJ.py*, which works by recombining the "parent" dataset FIDs in a specific way. In this study, the 2D projection spectra were zero-filled and windowed by a cosine-squared function in both dimensions. Linear prediction was applied to the indirect dimension. The set of projection spectra with different projection angles was then analyzed automatically by GAPRO[5] to generate a 4D peak list for sequential assignment.

To run the 4D experiments on TopSpin:

1. Create a 2D experiment and import the pulse program into **PULPROG**.
2. Adjust all shaped pulses' pulse length to values recommended in the pulse program (for 700 MHz spectrometer) and adjust the respective shaped pulse power accordingly.
3. Afterwards, run a test experiment with projection angles **α and β = 0**°, which is equivalent to 2D hncocaNH, to check sensitivity as well as to confirm that all pulses have been set correctly. For this experiment, **FnMODE = "Echo-Antiecho"** and **ZGOPTNS = "-DE5"**. Observe nucleus in F1 is set to 15N. This spectrum can be processed directly by the command ***xfb***.
4. To run the 4D HNcocaNH experiment, set the desired projection angles **0**° < **α, β** < **90**°. Set **FnMODE = "undefined"** and **ZGOPTNS = "-DE125"**. In this experiment, **TD1** should be set **4 times** the required TD1 of the projection spectra, *e.g.* **TD1 = "880"** if the desired TD1 for the projection spectra is 220. To run the 4D HNcocancaNH (x-P-x) experiment, **ZGOPTNS = "-DE125 -DPro"** and the additional shaped pulses will require adjustment of pulse length and power.
5. To generate the "child" datasets after acquisition, manually make four copies of the "parent" dataset, *e.g.* copy folder *1* into folders *101*, *102*, *103* and *104*. It is good to edit the followings: **$TD = 220** in the *acqu2s* file and **MC2 = "States"**, before making the copies into "child" datasets. Copy the python script ***apsy_HNMJ.py*** into the first folder, *i.e. 101*. Edit **TDin1** in *apsy_HNMJ.py* to the correct value, *i.e.* 220. Afterwards, rename the *ser* file in folder *101* to ***ser.old*** and run the python script. A total of four *ser* files named ***ser1*** to ***ser4*** will be generated. ***Ser1*** should replace the *ser* file in folder *101*, and so on. Now the projection spectra from *101* to *104* can be Fourier transformed by ***xfb*** on TopSpin. (*Note: if the processed spectrum is incorrect, edit apsy_HNMJ.py and change* ***dtype='<i4'*** *to* ***dtype='>i4'****. This byte order issue is computer-dependent.*)

6. Repeat step 5 for the remaining sets of projection angles.
7. After all projection spectra are processed properly, they can be analyzed by GAPRO. The required files are: ***gapro_098_linux***, ***experiment.gap***, ***parameter.gap***, and ***spectra.gap***, which should be obtainable from Sebastian Hiller. Copy these files into the first folder, *i.e.* folder *101*.
8. In *experiment.gap*, write **DimensionalityProjections: 2**, **DimensionalitySpace: 4**, **Experiment: HNMJ**.
9. In *parameter.gap*, set **Smin1** and **Smin2** (the minimum numbers of supports for peak generation) to ≥ 3 and $\leq$ the total numbers of projection spectra as included in *spectra.gap*. The higher the values the fewer false peaks will be generated.
10. In *spectra.gap*, write the following to include all projection spectra used for the analysis:

```
#4
/home/…/101/pdata/1/2rr   alpha=75.000 beta=25.000
/home/…/102/pdata/1/2rr   alpha=-75.000 beta=25.000
/home/…/103/pdata/1/2rr   alpha=75.000 beta=-25.000
/home/…/104/pdata/1/2rr   alpha=-75.000 beta=-25.000
#4
/home/…/201/pdata/1/2rr   alpha=15.000 beta=25.000
/home/…/202/pdata/1/2rr   alpha=-15.000 beta=25.000
/home/…/203/pdata/1/2rr   alpha=15.000 beta=-25.000
/home/…/204/pdata/1/2rr   alpha=-15.000 beta=-25.000
……
```

11. Execute the program *gapro_098_linux*, run option ***(s) Peak pick projection spectra in Expert-mode***, choose option ***(2) XWINNMR*** and do not use SNcompensation. After peak peaking is finished, run option ***(3) Run GAPRO with convergence (test version)***, and the 4D peaklist ***HNMJ.peaks*** will be generated eventually.
12. Delete the first five lines in *HNMJ.peaks* that start with #, and run the following awk to generate two separate 2D peaklists of ^{1}H and ^{15}N chemical shifts of connected amides:

    ```
    awk '{$2=$3="";printf $0"\n"}' HNMJ.peaks > HNMJ_MJ.peaks
    awk '{$4=$5="";printf $0"\n"}' HNMJ.peaks > HNMJ_HN.peaks
    ```

    These peaklists can be imported into CARA and mapped on the ^{15}N-HSQC spectrum for inspection.

13. The MATLAB script that performs matching of two pairs of $^{1}H^{N}$ and $^{15}N^{H}$ chemical shifts of correlated spin systems can be requested from the authors.

4. Protein expression and sample preparation

Residues 41-330 of human SLP-65 were cloned into a modified pET16b vector coding for a fusion protein with N-terminal His_7-tag and Tobacco etch virus (TEV) cleavage site. The construct was transformed into *E. coli* strain BL21(DE3) and expressed in M9 minimal medium at 25 °C by induction with 1 mM IPTG. The cells were harvested 6 hours after induction. ^{13}C,^{15}N-labeled protein was expressed in M9 minimal with $^{15}NH_4Cl$ as nitrogen source and $^{13}C_6$-D-glucose as carbon source.

The cell pellet from 1 L of expression culture was resuspended in 60 ml of lysis buffer (50 mM sodium phosphate, pH 8.0, 300 mM NaCl, 10 mM imidazole, 0.5 mM PMSF, 1 tablet Complete™-EDTA protease inhibitor mix (Roche)), lysed by ultrasonication, followed by centrifugation at 27000 x g at 4 °C for 45 minutes. The supernatant was loaded onto a 5 ml Ni-NTA Protino column (Macherey-Nagel) equilibrated with lysis buffer. After washing the column with lysis buffer supplemented with 30 mM imidazole the protein was eluted with the buffer containing 300 mM imidazole. Fractions containing the protein were dialyzed against TEV cleavage buffer (20 mM Tris/HCl, pH 8.0, 200 mM NaCl, 0.5 mM EDTA, 1 mM DTT, 0.5 mM PMSF) and digested at 20 °C with 2 µg TEV/100 µg of fusion protein. After digestion the released His_7-tag was removed by passing the reaction mix over another Ni-NTA Protino column. The flowthrough fractions containing the protein were combined, dialyzed against gelfiltration buffer (20 mM HEPES, pH 7.2, 150 mM NaCl) and purified by size exclusion chromatography on a HiLoad 16/60 SD 75 gel filtration column. The peak fractions were pooled and dialyzed against NMR buffer 1 (20 mM MES, pH 6.0, 150 mM NaCl, 1 mM Tris(2-carboxyethyl)phosphine, 0.5 mM Pefabloc (Roth)) or NMR buffer 2 (20 mM HEPES, pH 7.2, 50 mM NaCl, 1 mM Tris(2-carboxyethyl)phosphine, 0.5 mM Pefabloc (Roth)). The protein concentration was adjusted accordingly using 10 kDa MWCO concentrators (Vivascience). 3-5 % D_2O was added to the samples for locking, and 0.4 mM 4,4-dimethyl-4-silapentane-1-sulfonic acid (DSS) was added for chemical shift referencing. The samples at pH 6.0 and pH 7.2 were kept in a 3-mm normal and a 5-mm Shigemi NMR tubes, respectively.

^{13}C,^{15}N-labeled α-synuclein was expressed and purified as described previously[7]. Sample containing 0.3 mM protein in 50 mM HEPES, 100 mM NaCl at pH 7.4 was kept in a 3-mm NMR tube.

5. List of NMR experiments and acquisition parameters

All experiments were measured on 700 MHz (16.5 T) spectrometers equipped with Bruker's AVANCE III console and either conventional TCI cryoprobe or nitrogen-cooled Prodigy TCI cryoprobe.

The projection angle β scales the proportion of chemical shift evolution as well as the projected spectral width of the first indirect dimension by sin(β)[5,6]. This value should be kept small for better sensitivity and line width. We note that angles β between 18° and 28° were sufficient to discern peak positions and enable accurate chemical shift determination by GAPRO. We also notice that in general the precision of the generated 4D peaks correlates positively with the numbers of complex points in the indirect dimension.

Sample 1: 0.7 mM ^{13}C,^{15}N-labeled SLP-65_{41-330}, 20 mM MES, pH 6.0, 150 mM NaCl, 288 K

4D Sensitivity-enhanced HNcocaNH APSY					
Projection angles (α, β)	Recovery delay (d1), No. of scans (NS)	First indirect dimension			Total measurement time
		No. of complex points (TD1/2)	spectral width (SW1)	Total evolution time (t_{1max})	
(±75°, ±25°)	d1 = 1 s, NS = 12	110	25.5 ppm	60.7 ms	3 h 53 min
(±15°, ±25°)	—	—	—	—	—
(±45°, ±22°)	—	—	—	—	—
(±60°, ±28°)	—	—	—	—	—
(±30°, ±19°)	—	—	—	—	—
4D Sensitivity-enhanced HNcocancaNH (x-P-x) APSY					
(±75°, ±22°)	d1 = 0.9 s, NS = 140	60	25.5 ppm	33.1 ms	24 h
(±15°, ±22°)	—	—	—	—	—

Sample 2: 1.1 mM ^{13}C,^{15}N-labeled SLP-65_{41-330}, 20 mM HEPES, pH 7.2, 50 mM NaCl, 288 K

4D Sensitivity-enhanced HNcocaNH APSY					
Projection angles (α, β)	Recovery delay (d1), No. of scans (NS)	First indirect dimension			Total measurement time
		No. of complex points (TD1/2)	spectral width (SW1)	Total evolution time (t_{1max})	
(±75°, ±25°)	d1 = 0.9 s, NS = 16	105	25.5 ppm	60.0 ms	4 h 31 min
(±15°, ±25°)	—	—	—	—	—
(±45°, ±22°)	—	—	—	—	—
(±60°, ±28°)	—	—	—	—	—
4D Sensitivity-enhanced HNcocancaNH (x-P-x) APSY					
(±75°, ±22°)	d1 = 0.9 s, NS = 96	48	25.5 ppm	26.5 ms	13 h
(±15°, ±22°)	—	—	—	—	—

Sample 3: 0.6 mM ^{13}C,^{15}N-labeled SLP-$65_{41\text{-}330}$, 20 mM MES, pH 6.0, 150 mM NaCl, 288 K

3D experiment	Recovery delay (d1), No. of scans (NS)	First indirect dimension			Second indirect dimension			Total measurement time
		No. of complex points (TD1/2)	spectral width (SW1)	Total evolution time ($t1_{max}$)	No. of complex points (TD2/2)	spectral width (SW2)	Total evolution time ($t2_{max}$)	
HNCACB	d1 = 1 s, NS = 8	36	56 ppm	3.7 ms	81	21 ppm	54.3 ms	1 d 8 h
HNcaCO	d1 = 1 s, NS = 8	20	6 ppm	19.9 ms	125	21 ppm	83.8 ms	1 d 4 h

Amino acid-selective HSQC (MUSIC), recovery delay d1 = 1 s						
Name in Bruker's library	Observable $^{1}H^{N}$-$^{15}N^{H}$ correlation peaks	No. of scans (NS)	First indirect dimension			Total measurement time
			No. of complex points (TD1/2)	spectral width (SW1)	Total evolution time ($t1_{max}$)	
music_tavi_3d_2	Ala and Ala+1	12	39	22 ppm	25 ms	20 min
music_tavi_3d	Ala+1	12	—	—	—	20 min
music_lavia_3d	Val+1, Ile+1, Ala+1	12	—	—	—	20 min
music_ser_3d	Ser+1	24	—	—	—	40 min
music_de_3d	Asp+1	16	—	—	—	28 min
music_de_3d	Glu+1	16	—	—	—	28 min
music_fhyw_3d	Phe+1,His+1,Tyr+1	32	—	—	—	54 min

Sample 4: 0.3 mM ^{13}C,^{15}N-labeled α-synuclein, 50 mM HEPES, pH 7.4, 100 mM NaCl, 288 K

4D Sensitivity-enhanced HNcocaNH APSY					
Projection angles (α, β)	Recovery delay (d1), No. of scans (NS)	First indirect dimension			Total measurement time
		No. of complex points (TD1/2)	spectral width (SW1)	Total evolution time (t_{1max})	
(±75°, ±25°)	d1 = 0.95 s, NS = 16	110	25.5 ppm	60.7 ms	5 h
(±15°, ±25°)	—	—	—	—	—
(±45°, ±22°)	—	—	—	—	—
4D Sensitivity-enhanced HNcocancaNH (x-P-x) APSY					
(±75°, ±22°)	d1 = 1 s, NS = 140	60	25.5 ppm	33.1 ms	1 d 2 h

6. Other supporting figures

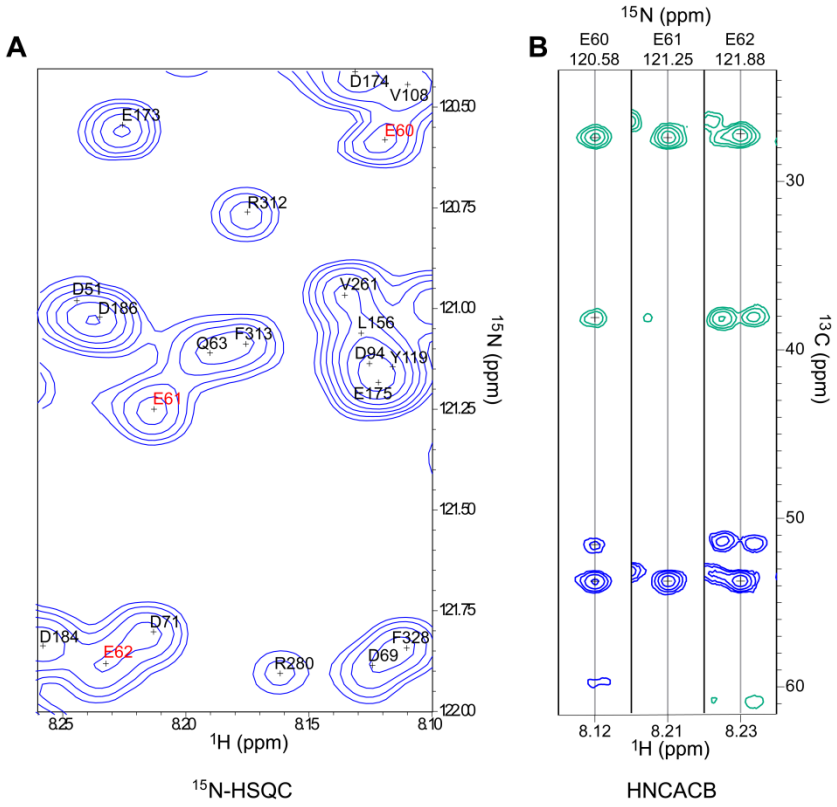

Figure S2. $^{1}H^{N}$-$^{15}N^{H}$ correlation peaks are well resolved. An example is shown to highlight the outstanding separation of $^{1}H^{N}$-$^{15}N^{H}$ correlation peaks of a repetitive sequence of the same amino acid (A), while their C^{α} and C^{β} peak positions on the ^{13}C dimension are overlapped in the HNCACB experiment (B).

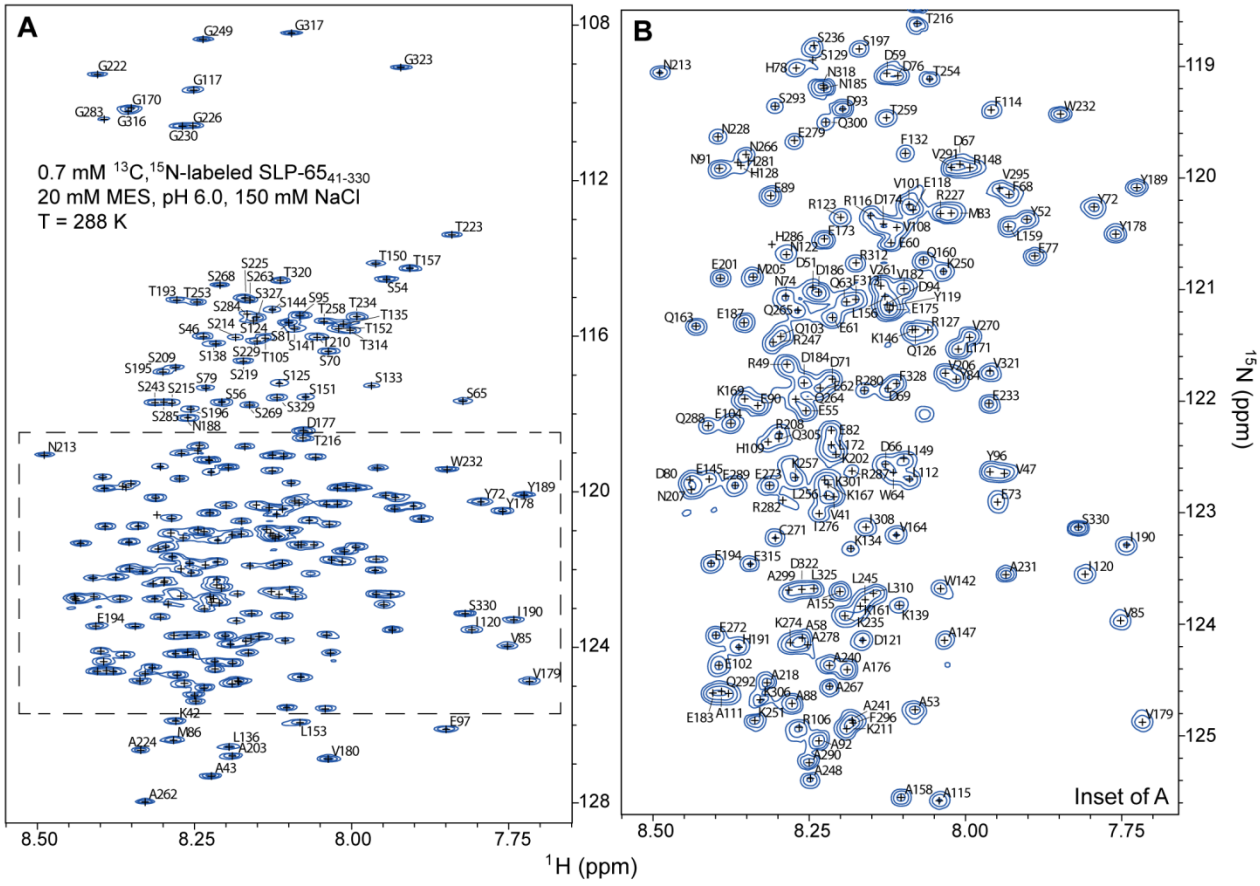

Figure S3. Assignment of SLP-65$_{41-330}$ at pH 6.0. (A) Residue-specific assignment of the amide resonances of SLP-65$_{41-330}$ at pH 6 and 288 K is shown on the HSQC spectrum. In (B), the spectrum is zoomed in for visual clarity.

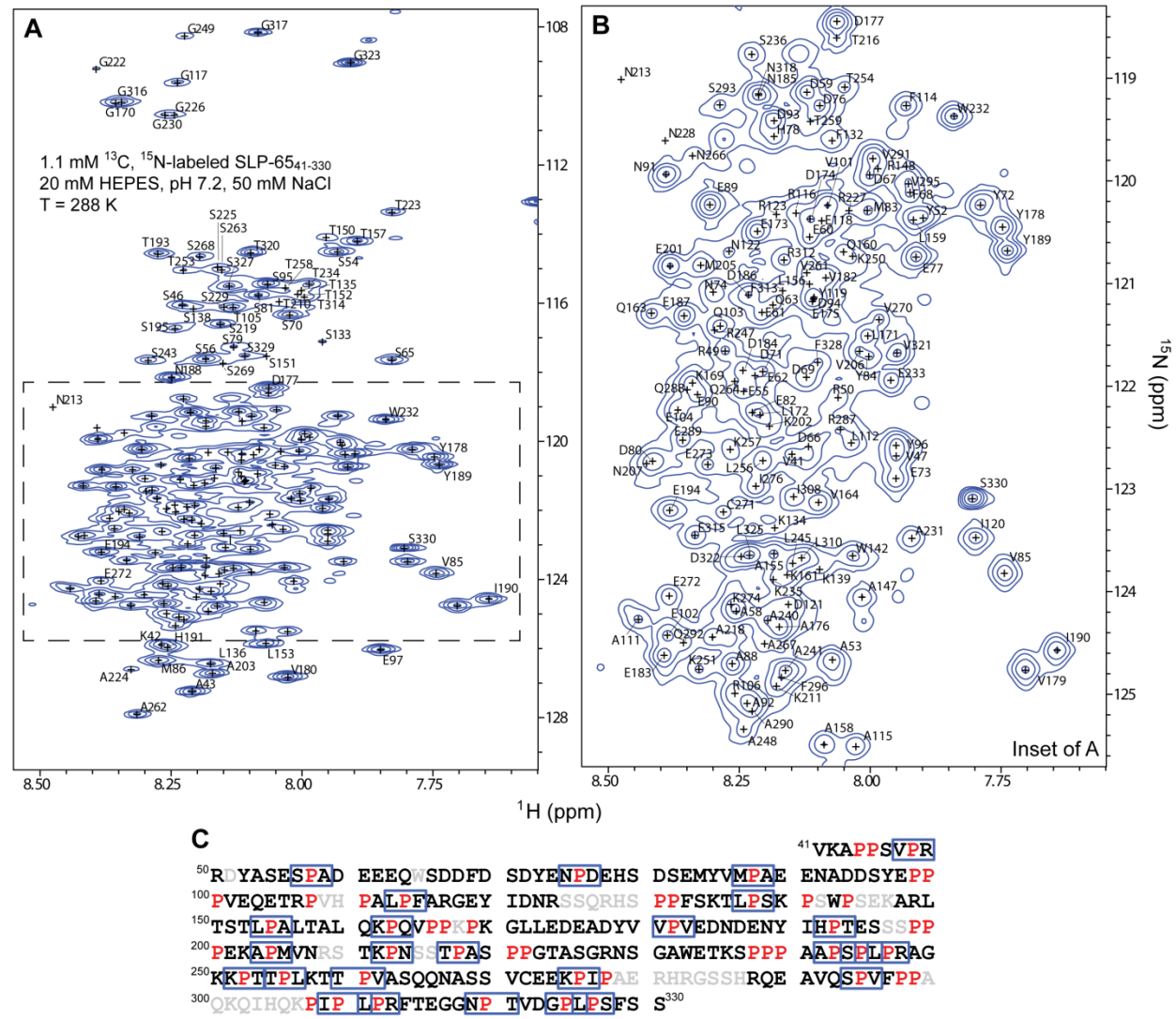

Figure S4. Assignment of SLP-65$_{41-330}$ at pH 7.2. (A) Residue-specific assignment of the amide resonances of SLP-65$_{41-330}$ at pH 7.2 and 288 K is shown on the HSQC spectrum. In (B), the spectrum is zoomed in for visual clarity. (C) Assigned (black), unassigned (gray), and prolyl (red) residues were colored differently on the amino acid sequence of SLP-65$_{41-330}$. x-P-x connectivity that were determined from the sensitivity-enhanced HNcocancaNH (x-P-x) experiment measured on this sample are highlighted by blue-colored boxes.

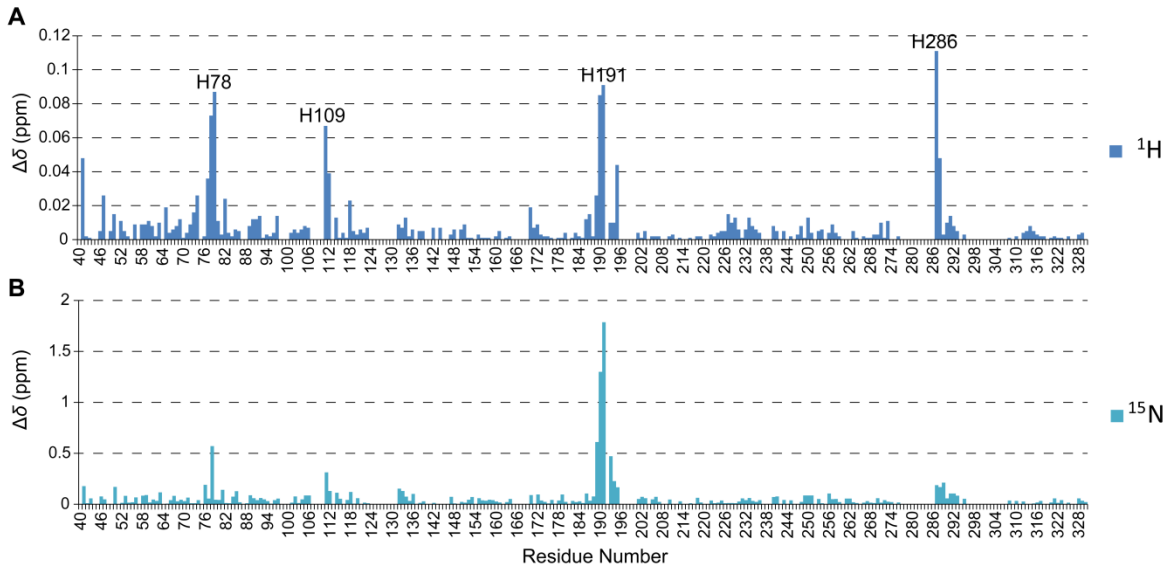

Figure S5. Differences in amide chemical shift between pH 6.0 and pH 7.2. Absolute value of the difference in amide $^{1}H^{N}$ chemical shifts (A) and $^{15}N^{H}$ chemical shifts (B) of SLP-$65_{41\text{-}330}$ between pH 6.0 and pH 7.2 at 288 K. The positions of H_{78}, H_{109}, H_{191} and H_{286} on the residue number axis are indicated.

7. References

(1) Cavanagh, J.; Palmer, A. G.; Wright, P. E.; Rance, M. *J Magn Reson* **1991**, *91*, 429.
(2) Palmer, A. G.; Cavanagh, J.; Wright, P. E.; Rance, M. *J Magn Reson* **1991**, *93*, 151.
(3) Kay, L. E.; Keifer, P.; Saarinen, T. *J Am Chem Soc* **1992**, *114*, 10663.
(4) Fiorito, F.; Hiller, S.; Wider, G.; Wuthrich, K. *J Biomol NMR* **2006**, *35*, 27.
(5) Hiller, S.; Fiorito, F.; Wuthrich, K.; Wider, G. *Proc Natl Acad Sci U S A* **2005**, *102*, 10876.
(6) Hiller, S.; Wider, G.; Wuthrich, K. *J Biomol NMR* **2008**, *42*, 179.
(7) Hoyer, W.; Antony, T.; Cherny, D.; Heim, G.; Jovin, T. M.; Subramaniam, V. *J Mol Biol* **2002**, *322*, 383.